# IKKβ acts as a tumor suppressor in cancer-associated fibroblasts during intestinal tumorigenesis

Charles K. Pallangyo,[1] Paul K. Ziegler,[1] and Florian R. Greten[1,2,3]

[1]Institute for Tumor Biology and Experimental Therapy, Georg-Speyer-Haus, 60596 Frankfurt am Main, Germany
[2]German Cancer Consortium (DKTK), 69120 Heidelberg, Germany
[3]German Cancer Research Center (DKFZ), 69120 Heidelberg, Germany

**Cancer-associated fibroblasts (CAFs) comprise one of the most important cell types in the tumor microenvironment. A proinflammatory NF-κB gene signature in CAFs has been suggested to promote tumorigenesis in models of pancreatic and mammary skin cancer. Using an autochthonous model of colitis-associated cancer (CAC) and sporadic cancer, we now provide evidence for a tumor-suppressive function of IKKβ/NF-κB in CAFs. Fibroblast-restricted deletion of *Ikkβ* stimulates intestinal epithelial cell proliferation, suppresses tumor cell death, enhances accumulation of $CD4^+Foxp3^+$ regulatory T cells, and induces angiogenesis, ultimately promoting colonic tumor growth. In *Ikkβ*-deficient fibroblasts, transcription of negative regulators of TGFβ signaling, including *Smad7* and *Smurf1*, is impaired, causing up-regulation of a TGFβ gene signature and elevated hepatocyte growth factor (HGF) secretion. Overexpression of Smad7 in *Ikkβ*-deficient fibroblasts prevents HGF secretion, and pharmacological inhibition of Met during the CAC model confirms that enhanced tumor promotion is dependent on HGF–Met signaling in mucosa of *Ikkβ*-mutant animals. Collectively, these results highlight an unexpected tumor suppressive function of IKKβ/NF-κB in CAFs linked to HGF release and raise potential concerns about the use of IKK inhibitors in colorectal cancer patients.**

The development of cancer is intimately regulated by the cross talk between tumor cells and the surrounding stromal cells, which are composed of inflammatory immune cells, vascular cells, and cancer-associated fibroblasts (CAFs; Hanahan and Coussens, 2012). CAFs are one of the most abundant cell types in different tumor entities; they originate from heterogeneous cell types with different molecular definitions but form a phenotypically distinct cell type (Öhlund et al., 2014). Accumulating evidence suggests CAFs can accelerate the growth and development of primary tumors, invasion, and metastasis directly and indirectly as they secrete classical growth factors (Elenbaas and Weinberg, 2001), facilitate inflammation (Andoh et al., 2007; Servais and Erez, 2013), promote angiogenesis (Orimo et al., 2005), modulate the extracellular matrix (ECM) and enhance stiffness (desmoplasia; Allen and Louise Jones, 2011), and stimulate stemness (Chen et al., 2014). They are also involved in metabolic reprogramming of the tumor microenvironment (Valencia et al., 2014), thus influencing all stages of tumorigenesis, as well as response to treatment (Crawford et al., 2009; Öhlund et al., 2014). Importantly, in colorectal cancer (CRC) a distinct set of genes specifically up-regulated in CAFs predicts poor prognosis (Calon et al., 2015). However, similarly to tumor-associated macrophages, CAFs show a high degree of plasticity and can also provide antitumorigenic functions. Genetic ablation of CAFs in preclinical models of pancreatic cancer has, surprisingly, resulted in more aggressively growing tumors and reduced survival (Özdemir et al., 2014; Rhim et al., 2014), underscoring the observation that CAFs have a much wider range of functions. It is not yet clear which factors induce and determine the different subtypes of CAFs or the signaling pathways involved between the different subtypes of CAFs and other cell types in the tumor microenvironment.

Fibroblasts respond to proinflammatory signals, including IL-1β, TNF, reactive oxygen species (ROS), and TGF-β (Pang et al., 1994; Gordon, 2000; Ogura et al., 2004; Yucel-Lindberg and Brunius, 2006; Toullec et al., 2010), and in turn produce a variety of chemokines and cytokines recruiting and activating leukocytes to sites of inflammation (Räsänen and Vaheri, 2010; Servais and Erez, 2013). Fibroblasts play a major role in facilitating the switch from acute resolving to chronic inflammation (Buckley et al., 2001; Zhang et al., 2011; Servais and Erez, 2013). Indeed, CAFs seem to express a proinflammatory NF-κB–dependent signature in tumor models of skin, mammary, and pancreatic cancer, as well as their cognate human counterparts (Erez et al., 2010). This signature consists of genes encoding proinflammatory

Correspondence to Florian R. Greten: greten@gsh.uni-frankfurt.de

Abbreviations used: AOM, azoxymethane; CAC, colitis-associated cancer; CAF, cancer-associated fibroblast; CLSM, confocal laser scanning microscopy; Col, collagen; CRC, colorectal cancer; DSS, dextran sulfate sodium; ECM, extracellular matrix; EMT, epithelial–mesenchymal transition; FCD, functional capillary density; HGF, hepatocyte growth factor.



The Rockefeller University Press $30.00
J. Exp. Med. 2015 Vol. 212 No. 13 2253–2266
www.jem.org/cgi/doi/10.1084/jem.20150576

chemokines and cytokines such as CXCL1, CXCL2, COX2, CYR61, IL-1β, IL-6, and OPN. In transplanted tumors, recruitment of macrophages, neovascularization, and tumor cell proliferation is dependent on NF-κB signaling in co-injected CAFs. Thus, the inflammatory infiltrates and proliferating mesenchymal cells in the tumor microenvironment presumably provide essential growth factors and signaling molecules in an NF-κB–dependent manner that could further support proliferation and invasion of transformed cells (Erez et al., 2010; Jung et al., 2010; De Boeck et al., 2013).

IKKβ-dependent activation of NF-κB confers various important protumorigenic functions during colonic tumorigenesis that are dependent on tumor stage and cell type. Whereas during tumor initiation NF-κB enhances Wnt signaling in intestinal epithelial cells (IECs; Schwitalla et al., 2013a), during tumor promotion it controls cell death (Greten et al., 2004). Moreover, during tumor progression, epithelial NF-κB is required for recruitment of myeloid cells and induction of epithelial–mesenchymal transition (EMT; Schwitalla et al., 2013a). In contrast, in myeloid cells, NF-κB controls the transcription of a variety of proinflammatory cytokines that enhance tumorigenesis in a paracrine manner (Karin, 2009; Schwitalla et al., 2013a).

Whereas the diverse tumor-promoting functions of NF-κB in both malignant and inflammatory immune cells have been proven in large number of murine tumor models, direct genetic evidence for the role of NF-κB in other components of the tumor microenvironment, particularly CAFs in autochthonous tumor models, is lacking. Here, we demonstrate that NF-κB signaling in CAFs surprisingly confers antitumorigenic functions and suppresses intestinal tumor growth.

## RESULTS

### Lack of *Ikkβ* in fibroblasts increases intestinal tumor size

To target fibroblasts and CAFs throughout intestinal tumorigenesis, we employed tamoxifen-inducible *Col1a2*Cre-ER$^{T2}$ mice that restrict Cre-mediated recombination to all fibroblastic cells (Zheng et al., 2002). Lineage tracing in *Col1a2*Cre-ER$^{T2}$;*Rosa26R*$^{CAG\text{-}tdTomato}$ (Fig. 1 A) mice confirmed recombination in subepithelial stromal cells in both untransformed intestine and colonic tumors using the azoxymethane (AOM)/dextran sulfate sodium (DSS)–induced model of colitis-associated tumorigenesis (CAC; Greten et al., 2004). Immunofluorescent staining confirmed widespread expression of collagen I and IV in *Col1a2*Cre-ER$^{T2}$-targeted cells in both unchallenged intestine and in AOM/DSS-induced tumors, but only partial overlap with vimentin, Fsp1, and α-SMA expression (Fig. 1 B). Recombination was not limited to the intestine and, in agreement with the original characterization of the mice (Zheng et al., 2002), we observed widespread RFP expression in other organs, including lung, liver, pancreas, kidney, and spleen (Fig. 1 C). Flow cytometric analysis confirmed that *Col1a2*Cre-ER$^{T2}$ mice target ∼80% of all PDGFRα$^+$ cells in the intestine, which express mesenchymal markers CD29 and CD44, but not PDGFRβ (Fig. 1, D–F). Importantly, we could not detect recombination in other stromal cells, such as CD45$^+$ leukocytes, Ter119$^+$ erythroid cells, CD31$^+$ endothelial cells, and EpCAM$^+$ epithelial cells (Fig. 1, D–F).

To examine the effect of IKKβ-dependent NF-κB activation in CAFs during intestinal tumorigenesis, we crossed conditional *Ikkβ*$^{F/F}$ mice with *Col1a2*Cre-ER$^{T2}$ mice, and *Ikkβ* deletion was confirmed in intestinal vimentin$^+$ fibroblasts isolated from *Col1a2*Cre-ER$^{T2}$;*Ikkβ*$^{F/F}$ animals (termed *Ikkβ*$^{\Delta Fib}$; Fig. 1, G and H), but not in respective splenocytes (Fig. 1 I) or sorted lamina propria CD45$^+$ cells (Fig. 1 J) upon tamoxifen administration. Loss of *Ikkβ* in fibroblasts did not cause any overt phenotype, and *Ikkβ*$^{\Delta Fib}$ mice remained healthy when kept on a tamoxifen-containing diet without further challenge. However, when we performed the CAC model, *Ikkβ*$^{\Delta Fib}$ animals were surprisingly not protected from tumor development and developed similar number of tumors as *Ikkβ*$^{F/F}$ littermate controls (Fig. 2 A). Moreover, absence of IKKβ in fibroblasts even strongly promoted tumor growth (Fig. 2 B), and *Ikkβ*$^{\Delta Fib}$ mice developed a higher number of larger tumors (Fig. 2, C–E). Increased tumor size was accompanied by an increased proliferation rate and decreased apoptotic activity in tumor cells from *Ikkβ*$^{\Delta Fib}$ mice (Fig. 2, F–I). Comparable results were also obtained in a model of sporadic tumorigenesis when we repetitively injected AOM without inducing DSS-mediated colitis (Fig. 2, J–L). Furthermore, when we assessed tumor vascularization before sacrifice on day 84 of the colitis-associated tumor model by in vivo confocal laser scanning microscopy (CLSM) blood vessel area and length in *Ikkβ*$^{\Delta Fib}$ tumors was significantly increased when quantified by functional capillary density (FCD; Fig. 2, M and N). Flow cytometric analysis of stromal cells confirmed a significant increase in CD45$^-$CD31$^+$ endothelial cells (Fig. 2 O). To quantify the number of fibroblasts in the colon, we used the receptor tyrosine kinase PDGFRα as a marker due to its expression in >90% of fibroblast-like cells (Erez et al., 2010). Indeed, in *Ikkβ*$^{\Delta Fib}$ tumors, the number of EpCAM$^-$CD45$^-$PDGFRα$^+$ fibroblasts was markedly increased (Fig. 2 P), whereas the number of CD45$^+$ leucocytes remained unchanged (Fig. 2 Q). Immunohistochemical analysis of *Ikkβ* mutant tumors revealed significantly increased phosphorylation of Akt$^{S473}$ and Stat3$^{Y705}$ and increased nuclear β-catenin in tumor cells (Fig. 2, R–Z). Collectively, these data suggested that lack of IKKβ in fibroblasts promotes tumorigenesis either because of an increase in the number of activated fibroblasts and/or elevated secretion of cytokines that were capable of activating Akt, Stat3, and Wnt signaling pathways that presumably control tumor cell proliferation and cell death (Cirri and Chiarugi, 2012).

### Increased *hepatocyte growth factor* (*Hgf*) gene expression in *Ikkβ*-deficient fibroblasts

To identify possible IKKβ-regulated factors that could be responsible for the paracrine stimulation of tumor cell proliferation and angiogenesis, we performed qPCR on purified

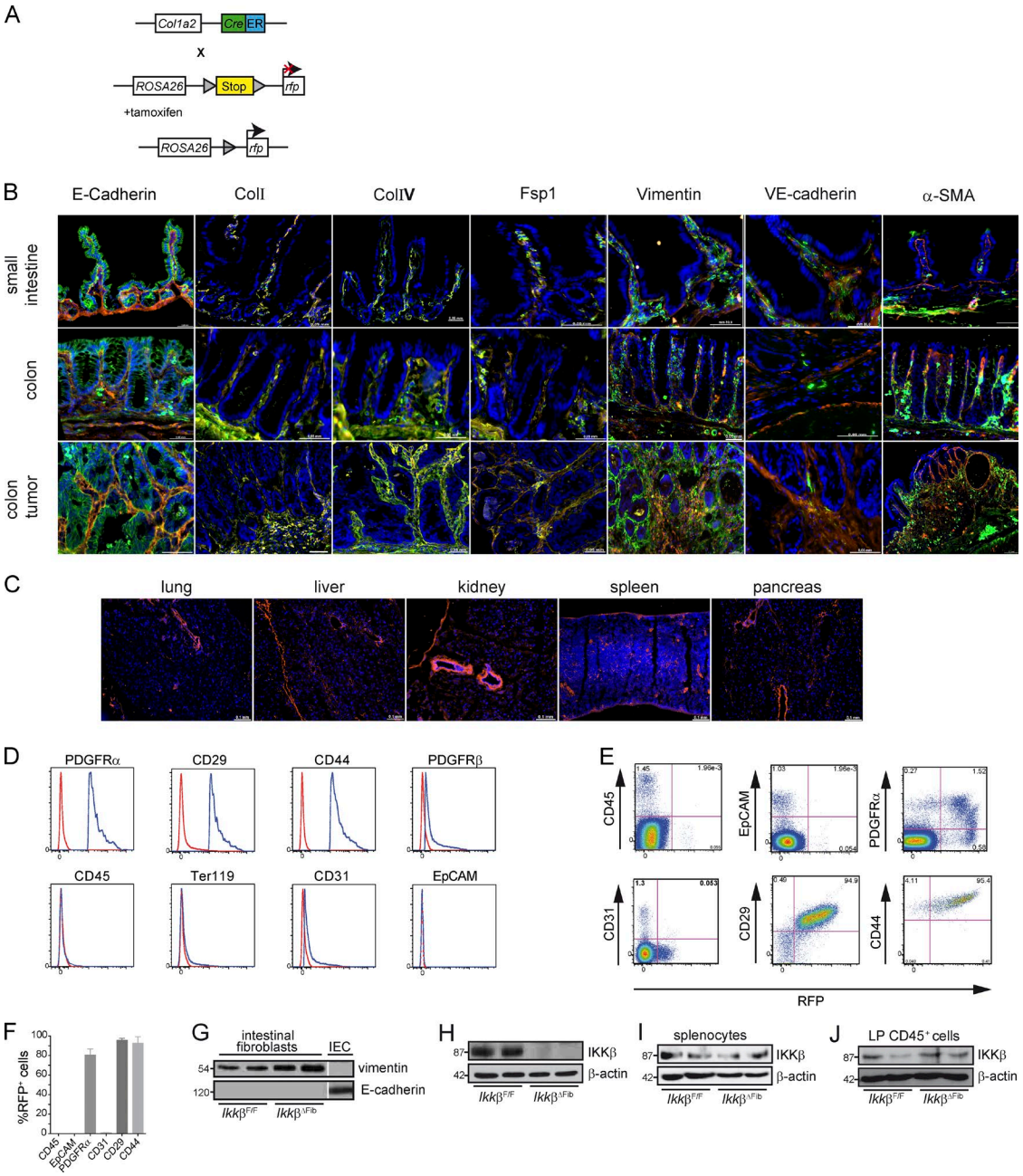


Figure 1. **Recombination in *Col1a2*Cre-ER$^{T2}$ mice is restricted to the fibroblast lineage and allows sufficient *Ikkβ* deletion in primary intestinal fibroblasts.** (A) Schematic representation of the genetic strategy used to generate mice for lineage tracing of the cells undergoing recombination. *Col1a2*Cre-ER$^{T2}$ mice crossed to a reporter mouse with a stop codon flanked by Cre-recombinogenic loxP sites upstream of a reporter gene for the red fluorescent protein (RFP) Tomato, under the control of the Rosa26 promoter to generate the compound mutant mouse *Col1a2*Cre-ER$^{T2}$;*Rosa26R*$^{CAG\text{-}tdTomato}$. After tamoxifen administration, Cre-recombinase excises the stop codon and Rosa26 drives expression of RFP. (B) Frozen tissue sections were stained for RFP (red) and the indicated markers (green). The cells coexpressing RFP and mesenchymal markers were marked yellow and were observed in the small intestine, colon in untreated mice, and colon tumors in AOM/DSS-treated mice. Nuclei are stained blue with DAPI. Bars, 50 µm. (C) RFP expression was also widely observed in other tissues, including lung, liver, kidney, spleen, and pancreas. Nuclei are stained blue by DAPI. Bars, 100 µm. (D) Flow cytometry analysis of RFP-expressing cells in untreated *Col1a2*Cre-ER$^{T2}$;*Rosa26R*$^{CAG\text{-}tdTomato}$ mice using markers for immune cells (CD45), epithelial cells (EpCAM), erythroid cells (Ter119), endothelial cells (CD31), and mesenchymal cells (CD29, CD44, PDGFRα, and PDGFRβ) after tamoxifen (400 mg/kg) administration for 5 d to induce cre recombination. (E–F) Representative flow cytometric analysis to quantify number of CD45$^+$, EpCAM$^+$, PDGFRα$^+$, CD31$^+$, CD29$^+$, and CD44$^+$ cells in RFP$^+$ population. (D) Mean number of RFP$^+$ cells in respective cell populations. Data are mean ± SE; $n \geq 5$. (G) Immunoblot analysis confirming purity of isolated primary intestinal fibroblasts from 6–8-wk-old *Ikkβ*$^{\Delta Fib}$ and *Ikkβ*$^{F/F}$ mice that were placed on a diet containing tamoxifen (400 mg/kg) for 5 d to induce cre recombination. (H–J) Immunoblot analysis of IKKβ confirms selective deletion in fibroblasts (H) but not splenocytes (I) or lamina propria (LP) CD45$^+$ cells (J) from tamoxifen-treated *Ikkβ*$^{\Delta Fib}$ mice.

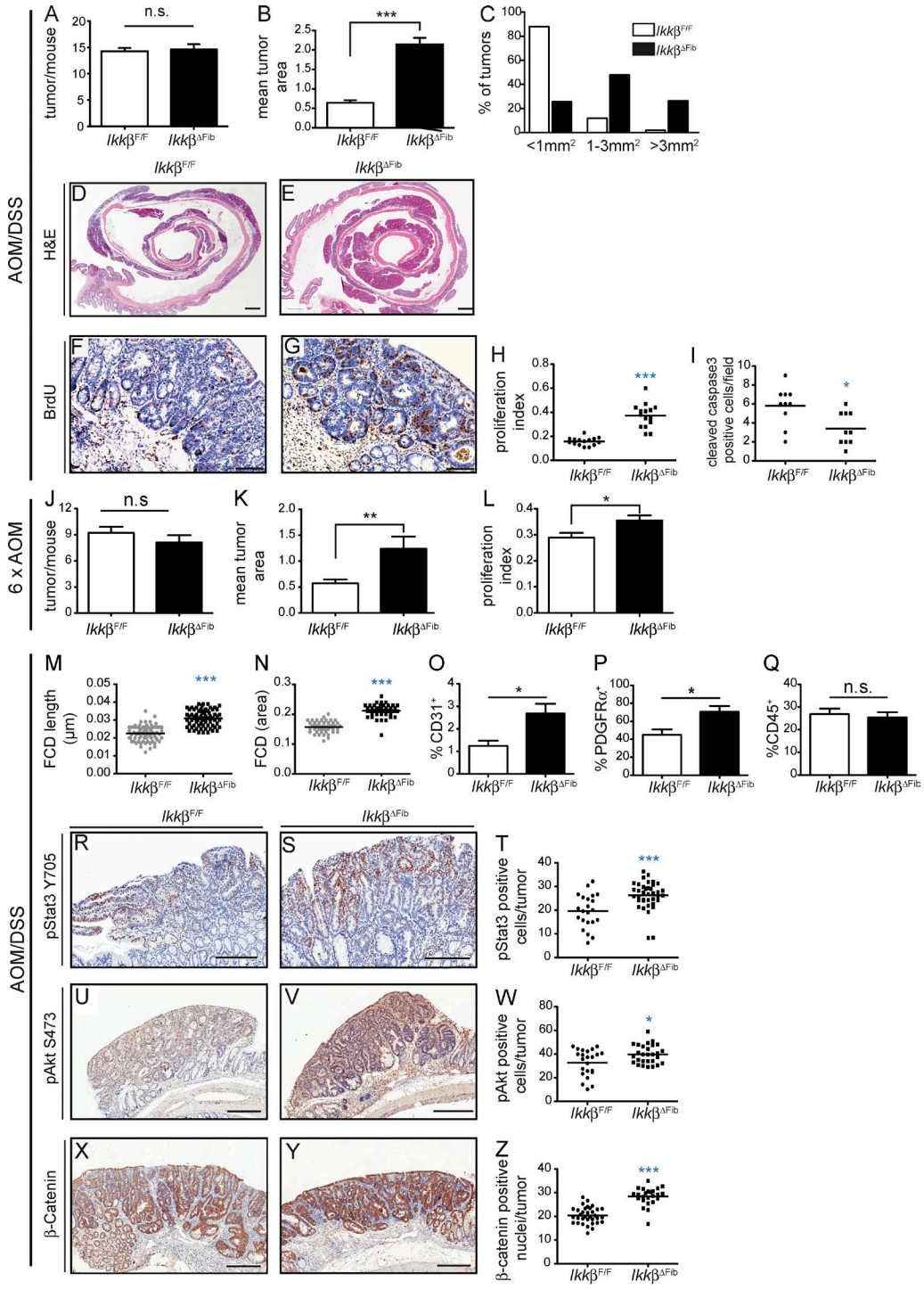


Figure 2. **Fibroblast-specific *Ikkβ* deletion promotes colon tumorigenesis.** (A) Tumor incidence in $Ikk\beta^{F/F}$ and $Ikk\beta^{\Delta Fib}$ mice at the end of the AOM/DSS regimen on day 84. Data are mean from two independent experiments ± SE; $n \geq 7$; ns, not significant. (B) Mean tumor size in $Ikk\beta^{F/F}$ and $Ikk\beta^{\Delta Fib}$ mice. Data are mean ± SE; $n \geq 7$; ***, $P < 0.0001$ by Student's *t* test. (C) Histogram showing size distribution of tumors in $Ikk\beta^{F/F}$ and $Ikk\beta^{\Delta Fib}$ mice. (D and E) Overview of representative sections of the Swiss rolls that were used for tumor counting; bars, 1 mm. (F–H) Immunohistochemical analysis of BrdU incorporation (F and G) and proliferation index (H) in tumor epithelial cells from $Ikk\beta^{F/F}$ and $Ikk\beta^{\Delta Fib}$ mice. Bars, 50 µm. (I) Quantification of cleaved caspase 3 staining for the apoptotic index in tumor epithelial cells from $Ikk\beta^{F/F}$ and $Ikk\beta^{\Delta Fib}$ mice. (J) Tumor incidence in $Ikk\beta^{F/F}$ and $Ikk\beta^{\Delta Fib}$ mice at the end of the sporadic tumor regimen (six weekly AOM injections without additional DSS administration) at week 22. Data are mean from two independent experiments ± SE; $n \geq 9$; ns, not significant. (K) Mean tumor size in $Ikk\beta^{F/F}$ and $Ikk\beta^{\Delta Fib}$ mice. Data are mean ± SE; $n \geq 9$; **, $P < 0.005$ by Student's *t* test. (L) Quantification of the prolifer-

EpCAM$^-$CD45$^-$PDGFR$\alpha^+$ CAFs sorted by flow cytometry from tumors of *Ikkβ*$^{\Delta Fib}$ and *Ikkβ*$^{F/F}$ mice. In line with a more activated phenotype of *Ikkβ*-deficient fibroblasts, *αSma*, *Fap*, and *Col1a* gene expression was markedly elevated, yet *Fgf1* or *bFgf* expression was comparable (Fig. 3 A). In contrast, transcription of genes encoding classical NF-κB–dependent proinflammatory cytokines, such as *Il6*, *Cox2*, *Cxcl1*, and *Cxcl12* was reduced, whereas *Il-1β*, *Cxcl2*, and *Cxcl5* expression levels remained unchanged (Fig. 3 A). CAFs are the main drivers of stromal TGF-β–driven programs associated with poor clinical outcome in CRC (Calon et al., 2014). We therefore examined gene expression levels of *Tgfb1*, *Tgfb2*, and *Tgfb3*, but could not detect any relevant changes in their expression levels between the different genotypes. However, *Smad7* and *Smurf1* coding for negative regulators of TGFβ signaling, and the former known to be transcriptionally regulated by NF-κB (Bitzer et al., 2000; Freudlsperger et al., 2013), were markedly down-regulated in the absence of IKKβ, causing up-regulation of several TGFβ-controlled targets, including *Decorin*, *Ctgf*, *Cald1*, *Postn*, *Il11*, and *Igfbp7* (Fig. 3 A). Importantly, however, *Hgf* mRNA coding for one of the most prominent promitogenic factors secreted by CAFs was markedly up-regulated (Fig. 3 A). HGF is a pleiotropic cytokine produced mainly by fibroblasts, and it acts on adjacent epithelial and endothelial cells by binding to cell surface c-Met receptor, promoting cell survival, proliferation, and migration via Akt, Stat3, and Wnt activation (Hoot et al., 2010; Nakamura et al., 2011; Organ and Tsao, 2011). HGF is also known to be a potent angiogenic factor, stimulating endothelial cell recruitment, motility, and growth (Bussolino et al., 1992; Trusolino et al., 2010). Overexpression of HGF or its receptor c-Met is seen in many tumors, including CRC, and is associated with poor prognosis (Stein et al., 2009; Liu et al., 2012). Accumulating evidence suggests a role of CAFs, and particularly HGF, in maintaining the cancer–stem cell niche (De Wever et al., 2008; Vermeulen et al., 2010; Quante et al., 2011). We therefore analyzed sorted EpCAM$^+$ tumor cells and detected consistent up-regulation of various cancer stem cell markers, including *Ascl2*, *Tnfrsf19*, *Sox2*, *Sox9*, *EphB2*, *EphB3*, *Dclk1*, and *Lgr5*, as well as EMT master regulators *Snail* and *Slug* in tumor cells derived from *Ikkβ*$^{\Delta Fib}$ mice, indicating increased stemness (Fig. 3 B). This strongly supported the possibility that the observed phenotype in *Ikkβ*$^{\Delta Fib}$ mice regarding increased IEC proliferation, increased angiogenesis, and stemness could be explained by elevated HGF expression in *Ikkβ*-deficient fibroblasts.

### Enhanced IEC proliferation in response to acute colitis in *Ikkβ*$^{\Delta Fib}$ mice

To examine whether the decreased expression of proinflammatory cytokines in *Ikkβ*-deficient fibroblasts would affect the outcome of DSS-induced colitis, we examined animals of both genotypes on day 15 of the AOM/DSS model during the acute phase of inflammation. However, loss of *Ikkβ* in fibroblasts did not affect the initial DSS-induced epithelial cell death (not depicted), and therefore the extent of inflammation determined by weight loss (Fig. 4 A), histological damage, and number of ulcerations (Fig. 4, B and C) was indifferent between both genotypes. Whereas *Tnfa* and *Il1b* mRNA levels were not altered in *Ikkβ*$^{\Delta Fib}$ whole mucosa, *Il6* and *Cxcl1* expression was decreased (Fig. 4 D). Importantly, despite no differences in the mRNA levels of *Tgfb1*, *Tgfb2*, and *Tgfb3*, already at this early time point *Hgf* and *Fgf1* and *bFgf* gene expression was markedly elevated in mucosa of DSS-challenged *Ikkβ*$^{\Delta Fib}$ mice (Fig. 4 D). This was paralleled by increased epithelial Met phosphorylation in *Ikkβ*$^{\Delta Fib}$ mice (Fig. 4, E–H), which presumably was responsible for promoting IEC proliferation (Fig. 4, I–K). Myofibroblasts play an active role in regulation of the type and duration of leukocyte infiltration after acute inflammation (Pilling et al., 1999; Servais and Erez, 2013), and deregulation of this process can lead to inappropriate immune responses promoting tumorigenesis (Östman and Augsten, 2009). Fibroblasts can also suppress inflammation by inducing FoxP3$^+$ regulatory T cell proliferation directly by secreting TGF-β into the microenvironment (Yang et al., 2010) or in an IL-15–dependent manner (Clark and Kupper, 2007). We therefore isolated and analyzed the lamina propria–infiltrating immune cell populations during DSS-induced colitis by flow cytometry. Although we found no differences in the relative numbers of CD45$^+$, EpCAM$^+$, CD31$^+$, and PDGFR$\alpha^+$ cells (Fig. 5 A), or CD11b$^+$F4/80$^+$, CD11b$^+$Gr-1$^+$, and CD11b$^+$CD11c$^+$ myeloid cells (Fig. 5 B), we found a significant increase in the relative numbers of CD3$^+$CD4$^+$ T cells, as well as CD4$^+$Foxp3$^+$ regulatory T cells in the *Ikkβ*$^{\Delta Fib}$ group. There was also a slight increase in CD4$^+$IFN$\gamma^+$ T cells, but it was not significant, the levels of CD4$^+$IL17a$^+$ T cells remained unchanged between the two groups (Fig. 5 C).

### Enhanced HGF secretion in the absence of *Ikkβ* depends on Smad7 down-regulation

To examine whether elevated *Hgf* transcription was a direct cell autonomous effect of *Ikkβ* deletion in fibroblasts or an

ation index in *Ikkβ*$^{F/F}$ and *Ikkβ*$^{\Delta Fib}$ tumors. Data are mean ± SE; $n \geq 20$ tumors per genotype; *, $P < 0.05$ by Student's *t* test. (M and N) Quantification of blood vessel FCD length and area in tumors from fluorescein injected *Ikkβ*$^{F/F}$ and *Ikkβ*$^{\Delta Fib}$ mice by CLSM. Data are mean ± SE; $n \geq 6$. ***, $P < 0.0001$ by Student's *t* test. (O–Q) Quantitative analysis of EpCAM$^-$CD45$^-$CD31$^+$ endothelial cells (O), EpCAM$^-$CD45$^-$PDGFR$\alpha^+$ fibroblasts (P), and CD45$^+$ leukocytes (Q) in tumors from *Ikkβ*$^{F/F}$ and *Ikkβ*$^{\Delta Fib}$ mice analyzed by flow cytometry. Data are mean ± SE; $n \geq 6$. *, $P < 0.05$ by Student's *t* test. (R–T) Immunohistochemical analysis of p-Stat3$^{Y705}$ (R and S) and quantification (T) in tumor epithelial cells from *Ikkβ*$^{F/F}$ and *Ikkβ*$^{\Delta Fib}$ mice. Bar, 200 µm. (U–W) Immunohistochemical analyses of p-Akt$^{S473}$ (U and V) and quantification (W) in tumor epithelial cells from *Ikkβ*$^{F/F}$ and *Ikkβ*$^{\Delta Fib}$ mice. Bar, 300 µm. (X–Z) Immunohistochemical analysis of β-catenin (X and Y) and quantification (Z) of nuclear expression in tumor epithelial cells from *Ikkβ*$^{F/F}$ and *Ikkβ*$^{\Delta Fib}$ mice. Bars, 300 µm. Data in H, I, T, W, and Z are mean ± SE; $n \geq 10$ tumors of each genotype; *, $P < 0.05$; ***, $P < 0.0001$ by Student's *t* test.

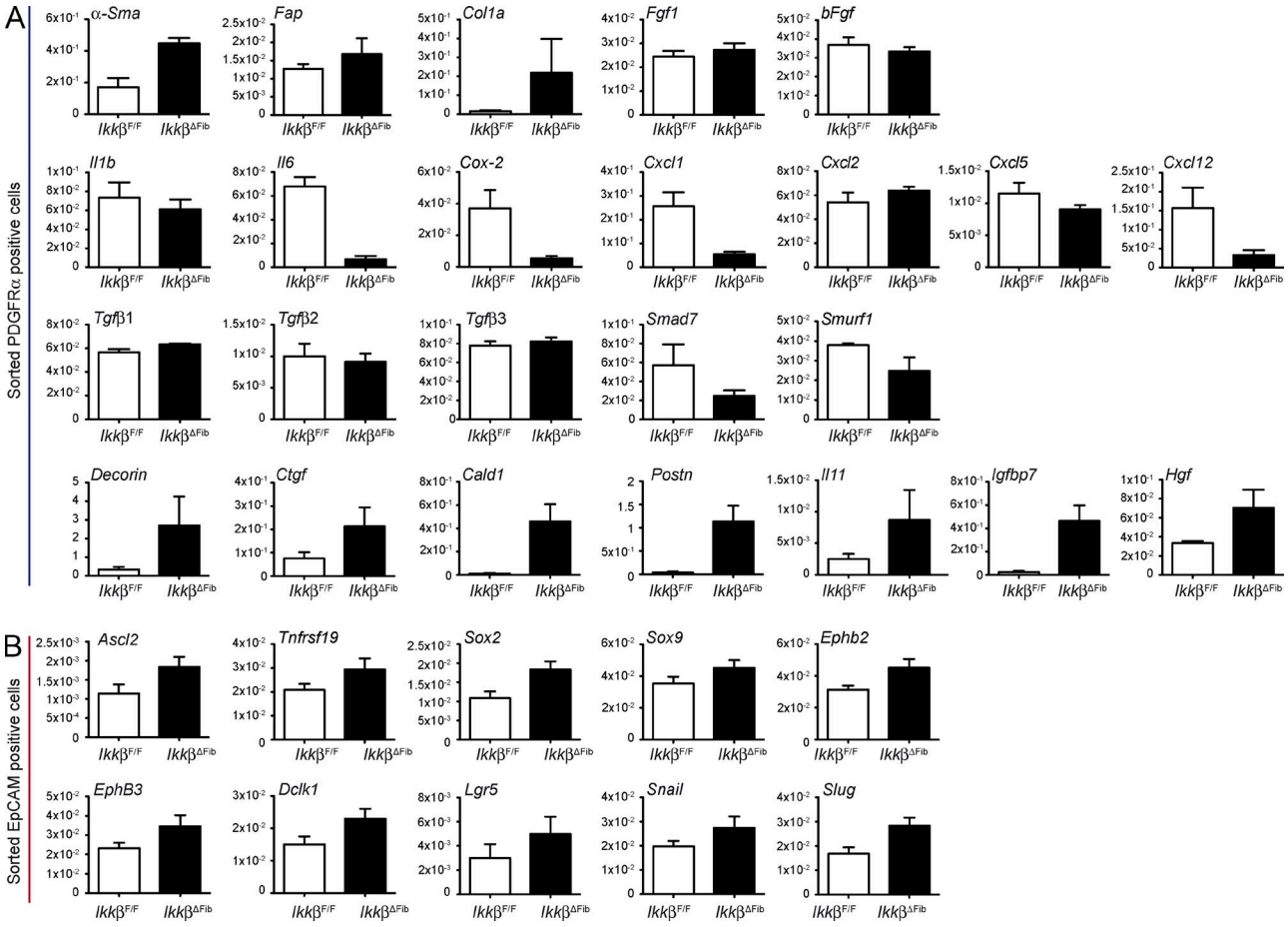


Figure 3. **Up-regulation of TGFβ-dependent transcriptional targets in *Ikkβ*-deficient CAFs.** (A) Relative expression levels of indicated mRNAs isolated from sorted PDGFRα$^+$ CAFs from AOM/DSS-induced tumor tissues of *Ikkβ*$^{F/F}$ and *Ikkβ*$^{\Delta Fib}$ mice and analyzed by real-time PCR. Data are mean from two independent experiments ± SE; $n \geq 4$. (B) Relative expression levels of indicated mRNAs isolated from sorted EpCAM$^+$ tumor cells from AOM/DSS-induced tumor tissues of *Ikkβ*$^{F/F}$ and *Ikkβ*$^{\Delta Fib}$ mice and analyzed by real-time PCR. Data are mean ± SE; $n \geq 4$.

indirect consequence by an altered microenvironment, we examined HGF production in purified ex vivo cultured intestinal fibroblasts. To this end, we purified intestinal fibroblasts from tumor-bearing *Ikkβ*$^{\Delta Fib}$ and *Ikkβ*$^{F/F}$ mice, as well as on day 15 of the CAC regimen. Fibroblasts were seeded in 24-well plates and cultured to 80% confluence. After 24 h of serum starvation, they were either left untreated or stimulated with TGFβ (10 ng/ml) or EGF (10 ng/ml) separately or simultaneously over a period of up to 72 h. Independent of the time point, whether cells had been isolated or the stimulus that had been applied, after DSS-induced colitis or AOM/DSS-induced tumorigenesis *Ikkβ*-deficient fibroblasts secreted up to fourfold more HGF compared with cells from littermate controls (Fig. 6, A and B). Similar effects were observed when cells were treated with PMA (unpublished data). These results clearly indicated that IKKβ directly suppresses HGF production in a cell autonomous manner. So far, NF-κB has not been shown to directly bind to the *Hgf* promoter, yet considering the clear induction by TGFβ in *Ikkβ*-deficient fibroblasts and the decreased *Smad7* expression in *Ikkβ*-deficient fibroblasts (Fig. 3 A), we speculated that IKKβ/NF-κB may affect HGF secretion via Smad7-dependent regulation of TGFβ signaling. Thus, using a retroviral approach, we overexpressed Smad7 in *Ikkβ*-deficient intestinal fibroblasts (Fig. 6 C), which indeed completely prevented TGFβ- and EGF-dependent HGF secretion in *Ikkβ*-deficient fibroblasts compared with cells that had been transduced with a GFP-control retrovirus (Fig. 6 D).

### Blocking c-Met signaling prevents tumor-promoting effects of *Ikkβ*-deficient fibroblasts

To finally confirm that enhanced HGF secretion by *Ikkβ*-deficient fibroblasts was responsible for the observed increase in tumor growth, we inhibited c-Met activation by feeding mice of both genotypes a diet containing a selective c-Met inhibitor INCB28060 (capmatinib; Liu et al., 2011) during the recovery phase after each DSS cycle (Fig. 7 A). Capmatinib did not affect tumor incidence, but blocked tumor

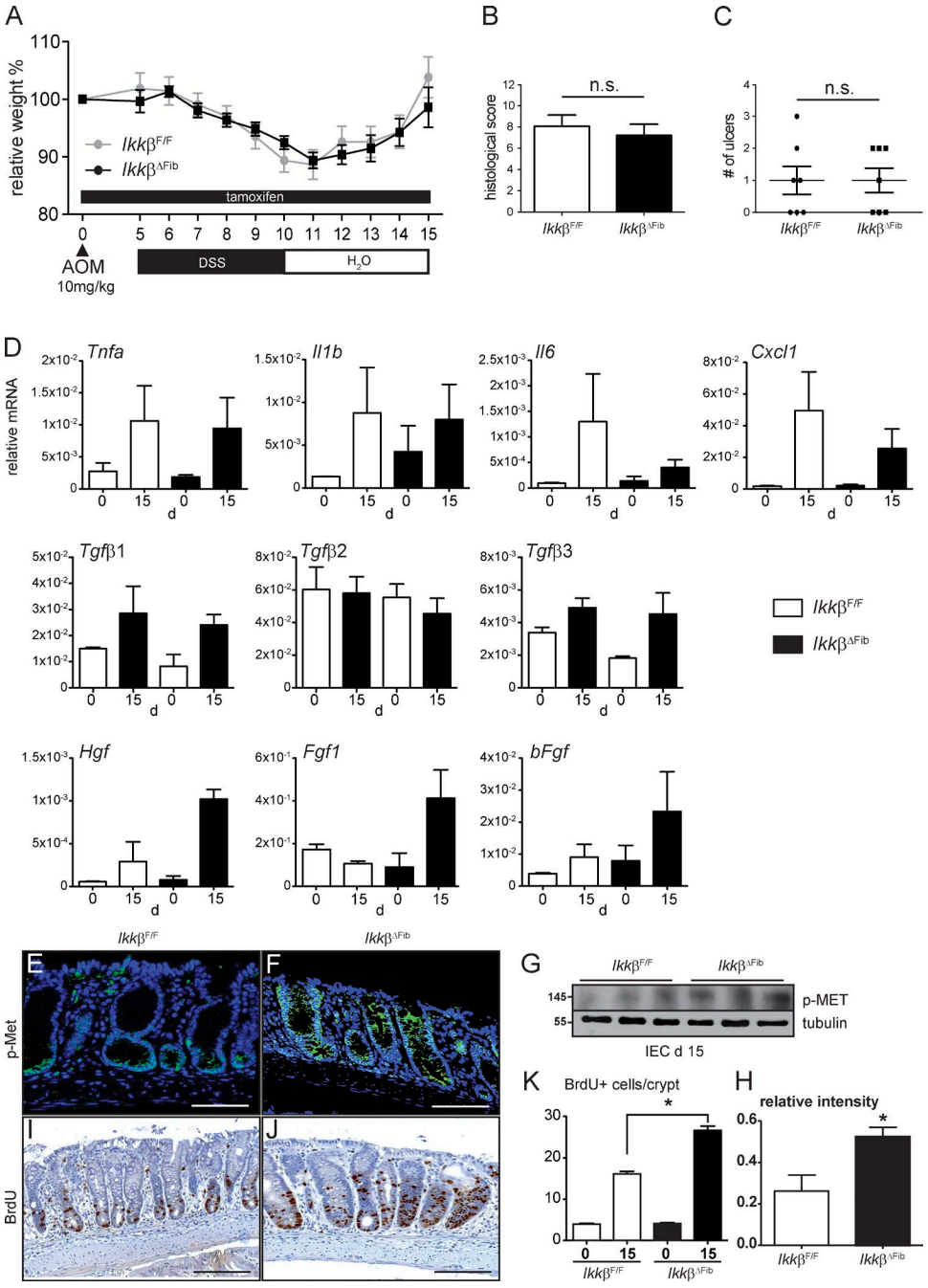


Figure 4. ***Ikkβ*-deficiency in fibroblasts does not affect inflammatory response, but stimulates IEC proliferation after acute DSS-induced colitis.** (A) Weight curves of *Ikkβ*$^{F/F}$ and *Ikkβ*$^{\Delta Fib}$ mice during first cycle of acute colitis. Data are mean from two independent experiments ± SEM. $n \geq 7$ mice per group. (B and C) Histological damage (B) and number of ulcerations (C) in *Ikkβ*$^{F/F}$ and *Ikkβ*$^{\Delta Fib}$ mice after the first cycle of DSS on day 15 of the AOM/DSS regimen. Data are mean ± SE; $n \geq 7$ mice per group. (D) Relative expression levels of indicated mRNAs isolated from whole mucosa of *Ikkβ*$^{F/F}$ and *Ikkβ*$^{\Delta Fib}$ mice on day 15 of the CAC model and analyzed by real-time PCR. Data are mean ± SE; $n \geq 7$. Data are mean from two independent experiments (E–G) Immunofluorescence staining of p-Met in whole mucosa (E and F) and immunoblot analysis of p-Met in IEC (G) of *Ikkβ*$^{F/F}$ and *Ikkβ*$^{\Delta Fib}$ mice on day 15 of the CAC model. (H) Quantification of immunoblot analysis using Image J. Bars, 20 µm. (I–K) Immunohistochemical analysis of BrdU incorporation (I and J) and proliferation index (K) in IEC (K) of *Ikkβ*$^{F/F}$ and *Ikkβ*$^{\Delta Fib}$ mice on day 15 of the CAC model. Bars, 20 µm. *, $P < 0.05$.

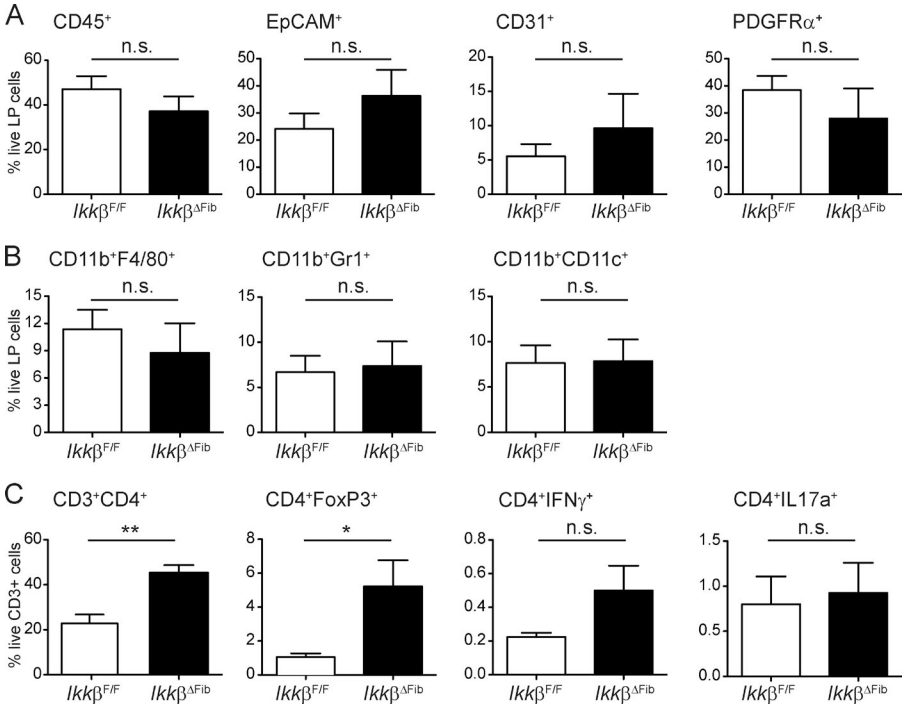


Figure 5. **Accumulation of CD4$^+$Foxp3$^+$ T cells in lamina propria of *Ikkβ*$^{\Delta Fib}$ mice on day 15 of the AOM/DSS model.** (A) Flow cytometric analysis of the colonic mucosa of *Ikkβ*$^{F/F}$ and *Ikkβ*$^{\Delta Fib}$ mice on day 15 of the CAC model revealed no difference in the numbers recruited CD45$^+$ immune cells, EpCAM$^+$ epithelial cells, CD31$^+$ endothelial cells or PDG FRα$^+$ fibroblasts at this time point. (B) Analysis of recruited myeloid cells showed no difference between the genotypes. (C) Analysis of CD4$^+$ T cell subsets showed significantly elevated numbers of total CD4$^+$ T cells and specifically CD4$^+$FoxP3$^+$ T reg cells in *Ikkβ*$^{\Delta Fib}$ mice. Data are mean from three independent experiments ± SEM. $n \geq 9$. *, $P < 0.05$; **, $P < 0.005$ by Student's *t* test.

growth in control animals (Fig. 7 B). However, in *Ikkβ*$^{\Delta Fib}$ mice, c-Met inhibition was even more apparent and capmatinib suppressed both tumor incidence, as well as tumor size. Two out of the eight treated *Ikkβ*$^{\Delta Fib}$ mice (25%) did not develop any adenomas, and capmatinib prevented the enhanced tumor growth in untreated *Ikkβ*$^{\Delta Fib}$ mice. Consequently, tumor size was now comparable to those in capmatinib-treated control animals. Moreover, capmatinib blocked angiogenesis in *Ikkβ*$^{\Delta Fib}$ mice to levels observed in *Ikkβ*$^{F/F}$ tumors (Fig. 7 D) and normalized the number of regulatory T cells in the mucosa during the acute inflammatory response (Fig. 7 H). In line with decreased tumor growth, activation of Stat3 and Akt and expression of nuclear β-catenin were down-regulated in the presence of capamatinib in *Ikkβ*$^{\Delta Fib}$ mice (Fig. 7, E–G). Collectively, these data confirmed that, indeed, enhanced HGF secretion by *Ikkβ*-deficient fibroblasts accounted for the enhanced tumor promotion in *Ikkβ*$^{\Delta Fib}$ mice by regulating tumor cell proliferation, cell death, angiogenesis, and T cell polarization.

## DISCUSSION

Canonical IKKβ-dependent NF-κB activation is considered a key signaling pathway linking inflammation and tumorigenesis (Greten et al., 2004). In tumor cells, as well as inflammatory immune cells, NF-κB controls a variety of functions that ultimately favor all stages of tumorigenesis (Karin, 2009). In line with this notion, CAFs in in pancreatic, skin, and mammary cancer express a proinflammatory NF-κB signature, and expression of dominant-negative IKKβ in cotransplanted CAFs inhibited tumorigenesis (Erez et al., 2010). Here, we report the unexpected observation that *Ikkβ* in Col1a2-expressing fibroblasts suppressed tumor growth in a model of CAC. This was strictly dependent on elevated HGF secretion, which stimulated cell proliferation, increased angiogenesis, and induced T reg cell polarization during colitis. Interestingly, pronounced HGF production was not limited to inflammation-associated tumorigenesis. We obtained similar results when sporadic colon tumors were initiated by AOM without additional DSS-triggered inflammation. The MAPK Tpl2 has been suggested to be involved in the upstream activation of NF-κB (Vougioukalaki et al., 2011). Interestingly, mice that lack *Tpl2* in ColVI expressing intestinal myofibroblasts show a very similar HGF-dependent phenotype in the CAC model, but not in an inflammation-independent model (Koliaraki et al., 2012). Surprisingly, however, IKKβ deletion in ColVI-expressing cells causes tumor inhibition in the CAC model, as discussed by Koliaraki and Kollias in this issue. Considering that Col1a2 targets nearly 80% of PDGFRα$^+$ cells, thus recombining in a much larger fraction of fibroblasts, raises the possibility that IKKβ/NF-κB may have distinct functions in different fibroblast subpopulations, possibly explaining the discrepancy between these results, as well as the previously reported findings when CAFs had been co-injected in xenografts of pancreatic and mammary cancer (Erez et al., 2010). Furthermore, the diametric opposite results in these two CAC studies here underscores the notion that CAFs represent much more than just one single cell type and provide strong evidence for the importance of different subpopulations within this cell lineage. Considering this high degree of plasticity in fibroblasts, NF-κB signaling may be differently affected or confer distinct functions depending on the respective activation status of CAF subpopulations.

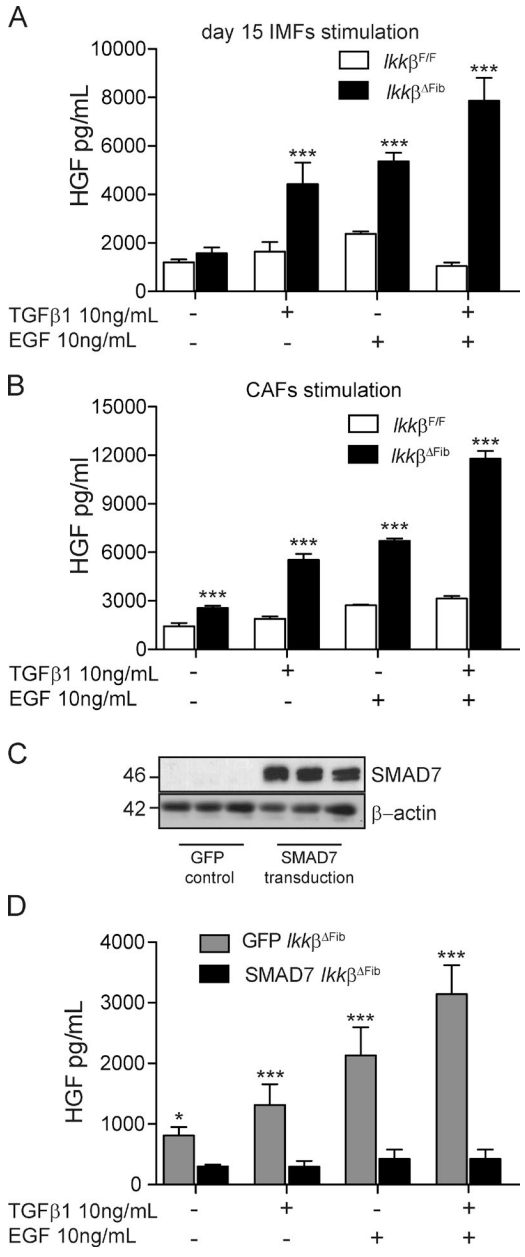


Figure 6. **Elevated HGF secretion in *Ikkβ*-deficient fibroblasts depends on Smad7.** (A) ELISA for HGF secreted by $Ikk\beta^{F/F}$ and $Ikk\beta^{\Delta Fib}$ fibroblasts. Primary fibroblasts were isolated from the colon on day 15 of the CAC model. Cells were seeded in 48-well plates and stimulated with 10 ng/ml TGFβ1 or EGF for 72 h. (B) ELISA for HGF secreted by $Ikk\beta^{F/F}$ and $Ikk\beta^{\Delta Fib}$ CAFs. Primary CAFs were isolated from AOM/DSS induced tumors. Cells were seeded in 48-well plates and stimulated with TGFβ1 10 ng/ml or EGF 10 ng/ml for 72 h. (C) Immunoblot analysis of Smad 7 in *Ikkβ*-deficient fibroblasts that had been retrovirally transduced with FLAG-tagged Smad7 or a GFP control. (D) Smad7 overexpression in *Ikkβ*-deficient fibroblasts prevents enhanced HGF secretion determined by ELISA. Data are mean ± SEM of three independent experiments performed in triplicate; $n \geq 4$ mice per group. *, $P < 0.05$; ***, $P < 0.0001$ by Student's *t* test.

Nevertheless, evidence emerging form other mesenchymal cell types, including adipocytes, macrophages, and muscle-derived stem cells NF-κB negatively regulates *Hgf* transcription in response to proinflammatory stimuli (Yin et al., 2014; Proto et al., 2015).

Our data further highlights the great importance of HGF for colorectal carcinogenesis. HGF is a potent and pleiotropic growth factor with important roles in regeneration and homeostasis in many adult tissues (Trusolino et al., 2010). It is secreted by mesenchymal cells, especially fibroblasts in a preform, and requires cleavage by extracellular proteases to produce the biologically active heterodimer, which can then bind to its receptor c-Met and activate downstream signaling. The C-terminal motif of c-Met contains docking sites for numerous downstream signaling pathways, including PI3K, GAB1, phospho-lipase Cγ1, and STAT3 (Ponzetto et al., 1994; Trusolino et al., 2010), leading to cell proliferation, reduced apoptosis, and enhanced angiogenesis. HGF has also been identified as the stromal factor responsible for maintenance of the cancer stem cell niche (Vermeulen et al., 2010) and aberrant activation of this signaling pathway correlates with a poor prognosis in CRC (Arlt and Stein, 2009). Indeed, sorted tumor cells from $Ikk\beta^{\Delta Fib}$ mice expressed higher levels of several stem cell and EMT markers. Interestingly, HGF seemed to be also responsible for T reg cell polarization during acute colitis considering the normalization upon capmatinib administration. This is consistent with findings in preclinical models of autoimmune diseases such as osteoarthritis, autoimmune myocarditis, and in CNS demyelinating autoimmune diseases when HGF promoted T reg cell accumulation by suppressing dendritic cell function (Okunishi et al., 2007; Benkhoucha et al., 2010).

One important upstream regulator of HGF secretion in CAFs is TGF-β. TGF-βRII–deficient fibroblasts secrete elevated levels of HGF, and fibroblast-specific deletion of TGF-βRII triggers development of spontaneous prostate and forestomach cancer (Bhowmick et al., 2004). In squamous cell carcinoma (SCC), it has been shown that HGF signaling is the central mediator of myofibroblast-derived paracrine signaling promoting tumorigenesis after TGF-β-dependent fibroblast to myofibroblast conversion. SCC cells produce TGF-β, thus activating adjacent fibroblasts, and the resulting myofibroblasts produced more HGF than their precursors, which significantly promoted tumor invasion (Lewis et al., 2004). We found TGFβ1 induces HGF secretion at significantly higher levels after genetic ablation of NF-κB signaling, and we could demonstrate that SMAD7 plays a key role in the control of HGF secretion in murine CAFs. SMAD7 negatively regulates TGFβ signaling, whereas it is transcriptionally regulated by NF-κB (Baugé et al., 2008; Yan et al., 2009; Freudlsperger et al., 2013). Cross talk between NF-κB and TGFβ signaling via SMAD7 has already been described in head and neck cancer (Freudlsperger et al., 2013), osteosarcoma (Eliseev et al., 2006), and breast and gastric cancers (Hong et al., 2007).

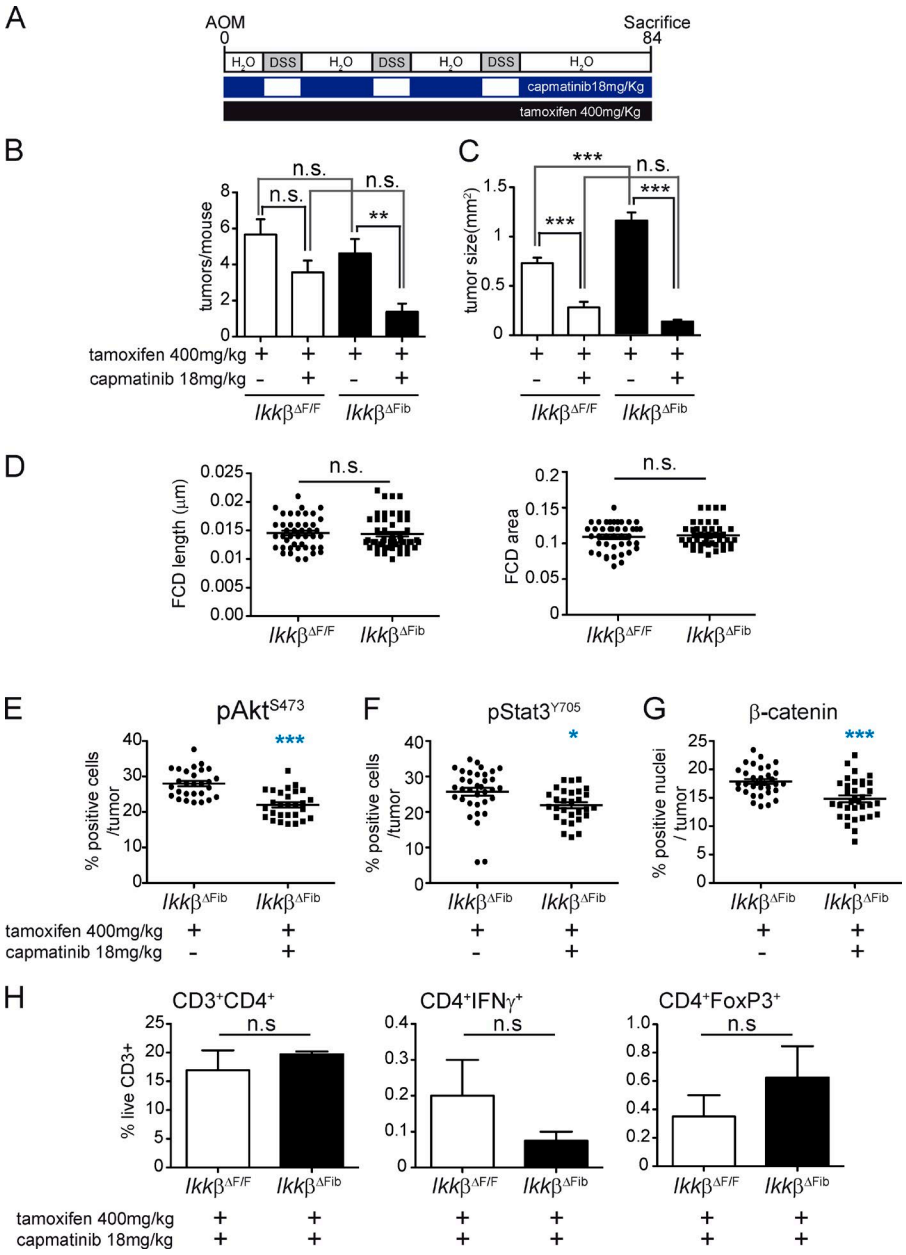


Figure 7. **Met inhibition prevents tumor promotion in *Ikkβ*$^{\Delta Fib}$ mice upon CAC challenge.** (A) Schematic overview of the CAC model and mode of capmatinib application. During DSS administration, capmatinib was paused and mice received tamoxifen containing AIN-76A diet. (B and C) Tumor incidence (B) and average tumor size (C) in *Ikkβ*$^{F/F}$ and *Ikkβ*$^{\Delta Fib}$ mice at the end of the AOM/DSS regimen that received capmatinib or were left untreated. Data are mean ± SE; $n \geq 7$; **, $P < 0.005$; ***, $P < 0.0001$ by ANOVA, followed by Bonferroni post hoc test for multiple datasets. (D) Quantification of blood vessel FCD length and area in tumors from capmatinib-treated *Ikkβ*$^{F/F}$ and *Ikkβ*$^{\Delta Fib}$ mice by CLSM. Data are mean ± SE; $n \geq 6$; ns, not significant. (E) Quantification of immunohistochemical analysis of p-Akt$^{S473}$ in tumor epithelial cells from untreated and capmatinib treated *Ikkβ*$^{\Delta Fib}$ mice. (F) Quantification of immunohistochemical analysis of p-Stat3$^{Y705}$ in tumor epithelial cells from untreated and capmatinib-treated *Ikkβ*$^{\Delta Fib}$ mice. (G) Quantification of immunohistochemical analysis of nuclear β-catenin in tumor epithelial cells from untreated and capmatinib-treated *Ikkβ*$^{\Delta Fib}$ mice. Data in E–G are mean ± SE; $n \geq 10$ tumors of each genotype; *, $P < 0.05$; ***, $P < 0.0001$ by Student's *t* test. (H) Flow cytometric analysis of lamina propia lymphocytes in *Ikkβ*$^{F/F}$ and *Ikkβ*$^{\Delta Fib}$ mice on day 15 of the CAC model revealed no difference in the numbers recruited CD3$^+$CD4$^+$, CD4$^+$FoxP3$^+$, and CD4$^+$IFNγ$^+$ when the mice received a diet containing the Met inhibitor capmatinib together with tamoxifen. Data are mean ± SE; $n \geq 7$ mice per group; ns, not significant.

Importantly, the enhanced TGFβ signaling in IKKβ-deficient CAFs did not just promote HGF release, but also led to the up-regulation of several other TGFβ-dependent target genes that have recently been identified to predict poor prognosis in CRC patients (Calon et al., 2015). Thus, in addition to the previously identified negative regulation of IL-1β secretion causing increased susceptibility to sepsis when inhibiting IKKβ (Greten et al., 2007), our data here raise additional concern regarding the use of specific IKKβ inhibitors for the treatment of CRC. However, considering that these effects seem to be restricted to CAFs, and that in intestinal tumor cells and myeloid cells NF-κB clearly confers tumor-promoting functions (Greten et al., 2004; Schwitalla et al., 2013a,b), it remains to be determined what net effect pharmacological IKKβ inhibition may have.

## MATERIALS AND METHODS

**Mice.** *Col1a2-cre*ER$^{T2}$ mice and *Rosa26R-tdTomato* reporter mice were purchased form The Jackson Laboratory. *Ikkβ*$^{F/F}$ have been described previously (Greten et al., 2004). All mice including cre-negative littermate controls were crossed on a FVB background for at least four generations and in all experiments littermate controls were used. To ensure sustained recombination mice were kept on a diet containing tamoxifen (400 mg/kg; LASvendi) throughout the duration of the CAC model. AOM/DSS-induced tumori-

genesis was performed essentially as previously described (Bollrath et al., 2009). 10 mg/kg AOM (Sigma-Aldrich) was injected i.p. at day 0, 5 d before mice received 2% DSS (MP Biosystems) in the drinking water for 5 d, followed by 16 d of regular water, which was repeated twice. Severity of colitis was assessed histologically as described before (Eckmann et al., 2008). The c-Met inhibitor INCB28060 (capmatinib) was purchased from Selleckchem and incorporated (18 mg/kg) along with tamoxifen (400 mg/kg) into rodent diet AIN-76A (Research Diets, Inc.). Control groups received tamoxifen containing AIN-76A diet only. All experiments were approved by the Regierungspräsidium Darmstadt.

**Histology and immunohistochemistry.** Colons were removed, opened longitudinally, rolled as swiss rolls, and fixed in 4% PFA overnight at 4°C. Tissues were subsequently dehydrated and paraffin embedded. 4 µm sections were used for histological analysis. For immunohistochemistry: after deparaffinization and rehydration of the tissue, antigen retrieval was done by incubating the tissue section in 10 mM sodium citrate buffer, pH 7.4 in sub boiling temperature in the microwave for 20 min. After cooling and washing the tissue, the endogenous peroxidase activity was quenched with 3% hydrogen peroxidase for 10 min at room temperature. Sections were blocked with 5% normal donkey serum in PBS containing 1% BSA and 0.1% Tween-20 for 1 h at room temperature. Endogenous avidin and biotin were blocked using the avidin-biotin kit (Vector Labs), following the manufacturer's instructions. The following primary antibodies were used: α-BrdU (MCA2060; AbDSerotec), α-cleaved caspase 3 (9661S; Cell Signaling Technology), α-p-Stat3$^{Y705}$ (9145; Cell Signaling Technology), α-pAkt$^{S473}$ (3787S; Cell Signaling Technology), α-β-catenin (06–734; EMD Millipore), α-p-Met (ab5662; Abcam), α-E-cadherin (610182; BD). To determine cell proliferation, mice were injected i.p. with 75 mg/kg BrdU (Sigma-Aldrich) 90 min before sacrifice. Quantification of positive nuclei was done using eSlide manager version 12.0.1.5027 after image acquisition by the Aperio Scanscope XT (Leica).

**Isolation of primary intestinal fibroblasts.** Colons were harvested and thoroughly washed with PBS containing 100 U/ml penicillin/streptomycin and 50 µg/ml gentamicin sulfate. For isolation of fibroblasts on day 15 of the AOM/DSS regimen, the entire distal one-third of the colon was harvested. For isolation of CAFs only tumor tissue was harvested and used for cell separation. After repeated washing, tissue was minced and digested in 1 mg/ml collagenase I (Sigma-Aldrich), 1 mg/ml Dispase II (Roche), 50 µg/ml DNase (Sigma-Aldrich) in 10 ml RPMI containing 2% FBS for 60 min. Supernatant was filtered through a 40-µM cell strainer, and the single-cell suspension was plated on T75 flasks. Cells were cultured in complete DMEM containing 10% FCS, 1% glutamax, 1% nonessential amino acids, 1% penicillin/streptomycin. Cells between the fourth and eighth passage were used for experiments. Cell stimulation was done after a 24-h serum starvation period and using DMEM containing only 1% PenStrep (Gibco), 1% glutamax (Gibco), and 1% nonessential Amino Acids (Gibco). For RNA analysis, cells were sorted by flow cytometry and directly collected in RNA lysis buffer.

**RNA and qPCR.** RNA from tissue/cells was harvested using RNeasy mini kit (QIAGEN). SuperScript II Reverse transcription (Life Technologies) was used for cDNA synthesis. qRT-PCR was then performed on a StepOne plus Real-Time PCR detection system (Applied Biosystems) using the SYBR Green PCR Master Mix (Roche) according to the manufacturer's instructions. Forward and reverse primers were added at a concentration of 0.2 pmol/ml in a final volume of 20 µl. The primers used are listed in Table S1.

**Protein analysis.** Immunoblotting was done using standard procedures. Protein lysates from cell pellets/tissue was separated using SDS-gel electrophoresis and transferred onto PVDF membranes. They were blocked with 5% milk in PBS containing 0.1% Tween 20 and incubated with specific antibodies. The following primary antibodies were used: α-p-Met (ab5662; Abcam) and α-SMAD-7 (sc-11392; Santa Cruz Biotechnology, Inc.). Secreted HGF in the supernatants was measured using an ELISA kit (R&D Systems) according to manufacturer's instructions.

**Flow cytometry.** Flow cytometry was performed using BD FACSCanto II flow cytometer, and analysis was done using Flow-Jo software, v8.8.6 (Tree Star). A schematic representation of the preparation and gating strategy is provided in. Fig. S1. Colon was harvested, washed thoroughly, minced using sterile scalpels, and digested in 1 mg/ml collagenase I (Sigma-Aldrich), 1 mg/ml Dispase II (Roche 04942078001), 50 µg/ml DNase (Sigma-Aldrich) in 10 ml of RPMI containing 2% FBS for 60 min. The supernatant was passed through a 40 µm cell strainer and the single cell suspension was stained using following antibodies: α-CD3 APC-eFluor 780(47–0032), α-CD4 eFluor 450(48–0041), α-CD8a PerCP-Cyanine5.5 (45–0081), α-IFN-κ Alexa Fluor 488(53–7311), α-IL-4 PE-Cyanine7 (25–7041), α-IL-17A APC (17–7177), α-Foxp3 PE (12–4771), α-CD11b APC-eFluor 780 (47–0112), α-CD11c FITC (11–0114), α-F4/80 APC (17–4801), α-Ly-6G (Gr-1) PE-Cyanine7 (25–5931), α-PDGFRα PE (12–1401-81), Fixable Viability Dye eFluor 506 (65–0866; all antibodies from eBioscience). For in vitro stimulation and intracellular staining, cells were plated on 6-well plates, stimulated with PMA (20 ng/ml) and ionomycin (1 µg/ml) in RPMI medium with 10% FCS and 1% PS and 1% Brefeldin A (eBioscience) for 5 h. Cells were then harvested and stained with specific antibodies for the surface markers and a fixable viability dye. The cells were then fixed using IC fixation buffer (eBioscience) and stained with antibodies for the intracellular stains in 1× wash/perm buffer.

**Confocal laser endomicroscopy.** Endoscopic imaging and quantification of angiogenesis was done using probe-based confocal laser endomicroscopy (CLE; CellVizio; Mauna Kea Technologies), enabling real-time in-vivo microscopy of mucosal surfaces. Anesthetized mice were injected with 10 µl of 1% fluorescein i.v. and, immediately after, examined with a miniprobe (Mauna Kea Technologies). CLE images were recorded as grayscale video sequence files at 12 frames per second for ten minutes 10 min after fluorescein injection. At least 10 images per tumor were used to calculate the FCD of the tumor areas ulsing the CellVizio software.

**Retrovirus production and retroviral transduction.** To prepare retroviral supernatants, pBabe Flag Smad7 plasmid (a gift from R. Derynck, University of California, San Francisco, CA; plasmid #14836; Addgene) was transfected into Phoenix-Eco packaging cells using the $CaPO_4$ transfection protocol. The virus-containing supernatant was collected 48 h after transfection. For retroviral transduction, one degree fibroblasts were plated in 6-well dishes at $2 \times 10^5$ cells (40–60%) confluence. After filtering and centrifugation, the virus supernatant containing 4 µg/ml polybrene was added and the cells were cultured for 48 h at 37°C. Selection of infected clones was done with puromycin. Control fibroblasts were transduced with eGFP retrovirus.

**Statistics.** Data are expressed as mean ± SEM. Statistical analysis methods used were standard two-tailed Student's *t* test for two datasets and ANOVA, followed by Bonferroni post-hoc test for multiple datasets using Prism4 (GraphPad). P-values ≤ 0.05 were considered significant.

**Online supplemental material.** Fig. S1 shows scheme of cell fractionation and confirmation of cell purity. Table S1, available as an Excel file, shows sequences of oligonucleotides used in real-time PCR. Online supplemental material is available at http://www.jem.org/cgi/content/full/jem.20150576/DC1.

## ACKNOWLEDGMENTS

We thank Natalia Delis, Kathleen Mohs, Christin Danneil, Eva Rudolf, and Petra Dinse for expert technical assistance.

This work was supported in part by the LOEWE Center for Cell and Gene Therapy Frankfurt (III L 4-518/17.004) and institutional funds from the Georg-Speyer-Haus, as well as grants from the Deutsche Forschungsgemeinschaft (Gr1916/11-1) and the ERC (ROSCAN-281967) to F.R. Greten.

The authors declare no competing financial interests.

**Submitted: 30 March 2015**
**Accepted: 3 November 2015**

## REFERENCES

Allen, M., and J. Louise Jones. 2011. Jekyll and Hyde: the role of the microenvironment on the progression of cancer. *J. Pathol.* 223:162–176. http://dx.doi.org/10.1002/path.2803

Andoh, A., S. Bamba, M. Brittan, Y. Fujiyama, and N.A. Wright. 2007. Role of intestinal subepithelial myofibroblasts in inflammation and regenerative response in the gut. *Pharmacol. Ther.* 114:94–106. http://dx.doi.org/10.1016/j.pharmthera.2006.12.004

Arlt, F., and U. Stein. 2009. Colon cancer metastasis: MACC1 and Met as metastatic pacemakers. *Int. J. Biochem. Cell Biol.* 41:2356–2359. http://dx.doi.org/10.1016/j.biocel.2009.08.001

Baugé, C., J. Attia, S. Leclercq, J.-P. Pujol, P. Galéra, and K. Boumédiene. 2008. Interleukin-1β up-regulation of Smad7 via NF-κB activation in human chondrocytes. *Arthritis Rheum.* 58:221–226. http://dx.doi.org/10.1002/art.23154

Benkhoucha, M., M.-L. Santiago-Raber, G. Schneiter, M. Chofflon, H. Funakoshi, T. Nakamura, and P.H. Lalive. 2010. Hepatocyte growth factor inhibits CNS autoimmunity by inducing tolerogenic dendritic cells and $CD25^+Foxp3^+$ regulatory T cells. *Proc. Natl. Acad. Sci. USA.* 107:6424–6429. http://dx.doi.org/10.1073/pnas.0912437107

Bhowmick, N.A., A. Chytil, D. Plieth, A.E. Gorska, N. Dumont, S. Shappell, M.K. Washington, E.G. Neilson, and H.L. Moses. 2004. TGF-β signaling in fibroblasts modulates the oncogenic potential of adjacent epithelia. *Science.* 303:848–851. http://dx.doi.org/10.1126/science.1090922

Bitzer, M., G. von Gersdorff, D. Liang, A. Dominguez-Rosales, A.A. Beg, M. Rojkind, and E.P. Böttinger. 2000. A mechanism of suppression of TGF-β/SMAD signaling by NF-κB/RelA. *Genes Dev.* 14:187–197.

Bollrath, J., T.J. Phesse, V.A. von Burstin, T. Putoczki, M. Bennecke, T. Bateman, T. Nebelsiek, T. Lundgren-May, O. Canli, S. Schwitalla, et al.. 2009. gp130-mediated Stat3 activation in enterocytes regulates cell survival and cell-cycle progression during colitis-associated tumorigenesis. *Cancer Cell.* 15:91–102. http://dx.doi.org/10.1016/j.ccr.2009.01.002

Buckley, C.D., D. Pilling, J.M. Lord, A.N. Akbar, D. Scheel-Toellner, and M. Salmon. 2001. Fibroblasts regulate the switch from acute resolving to chronic persistent inflammation. *Trends Immunol.* 22:199–204. http://dx.doi.org/10.1016/S1471-4906(01)01863-4

Bussolino, F., M.F. Di Renzo, M. Ziche, E. Bocchietto, M. Olivero, L. Naldini, G. Gaudino, L. Tamagnone, A. Coffer, and P.M. Comoglio. 1992. Hepatocyte growth factor is a potent angiogenic factor which stimulates endothelial cell motility and growth. *J. Cell Biol.* 119:629–641. http://dx.doi.org/10.1083/jcb.119.3.629

Calon, A., D.V.F. Tauriello, and E. Batlle. 2014. TGF-β in CAF-mediated tumor growth and metastasis. *Semin. Cancer Biol.* 25:15–22. http://dx.doi.org/10.1016/j.semcancer.2013.12.008

Calon, A., E. Lonardo, A. Berenguer-Llergo, E. Espinet, X. Hernando-Momblona, M. Iglesias, M. Sevillano, S. Palomo-Ponce, D.V.F. Tauriello, D. Byrom, et al.. 2015. Stromal gene expression defines poor-prognosis subtypes in colorectal cancer. *Nat. Genet.* 47:320–329. http://dx.doi.org/10.1038/ng.3225

Chen, W.-J., C.-C. Ho, Y.-L. Chang, H.-Y. Chen, C.-A. Lin, T.-Y. Ling, S.-L. Yu, S.-S. Yuan, Y.-J.L. Chen, C.-Y. Lin, et al. 2014. Cancer-associated fibroblasts regulate the plasticity of lung cancer stemness via paracrine signalling. *Nat. Commun.* 5:3472.

Cirri, P., and P. Chiarugi. 2012. Cancer-associated-fibroblasts and tumour cells: a diabolic liaison driving cancer progression. *Cancer Metastasis Rev.* 31:195–208. http://dx.doi.org/10.1007/s10555-011-9340-x

Clark, R.A., and T.S. Kupper. 2007. IL-15 and dermal fibroblasts induce proliferation of natural regulatory T cells isolated from human skin. *Blood.* 109:194–202. http://dx.doi.org/10.1182/blood-2006-02-002873

Crawford, Y., I. Kasman, L. Yu, C. Zhong, X. Wu, Z. Modrusan, J. Kaminker, and N. Ferrara. 2009. PDGF-C mediates the angiogenic and tumorigenic properties of fibroblasts associated with tumors refractory to anti-VEGF treatment. *Cancer Cell.* 15:21–34. http://dx.doi.org/10.1016/j.ccr.2008.12.004

De Boeck, A., A. Hendrix, D. Maynard, M. Van Bockstal, A. Daniëls, P. Pauwels, C. Gespach, M. Bracke, and O. De Wever. 2013. Differential secretome analysis of cancer-associated fibroblasts and bone marrow-

derived precursors to identify microenvironmental regulators of colon cancer progression. *Proteomics.* 13:379–388. http://dx.doi.org/10.1002/pmic.201200179

De Wever, O., P. Demetter, M. Mareel, and M. Bracke. 2008. Stromal myofibroblasts are drivers of invasive cancer growth. *Int. J. Cancer.* 123:2229–2238. http://dx.doi.org/10.1002/ijc.23925

Eckmann, L., T. Nebelsiek, A.A. Fingerle, S.M. Dann, J. Mages, R. Lang, S. Robine, M.F. Kagnoff, R.M. Schmid, M. Karin, et al.. 2008. Opposing functions of IKKβ during acute and chronic intestinal inflammation. *Proc. Natl. Acad. Sci. USA.* 105:15058–15063. http://dx.doi.org/10.1073/pnas.0808216105

Elenbaas, B., and R.A. Weinberg. 2001. Heterotypic signaling between epithelial tumor cells and fibroblasts in carcinoma formation. *Exp. Cell Res.* 264:169–184.

Eliseev, R.A., E.M. Schwarz, M.J. Zuscik, R.J. O'Keefe, H. Drissi, and R.N. Rosier. 2006. Smad7 mediates inhibition of Saos2 osteosarcoma cell differentiation by NFκB. *Exp. Cell Res.* 312:40–50.

Erez, N., M. Truitt, P. Olson, S.T. Arron, and D. Hanahan. 2010. Cancer-associated fibroblasts are activated in incipient neoplasia to orchestrate tumor-promoting inflammation in an NF-κB-dependent manner. *Cancer Cell.* 17:135–147.

Freudlsperger, C., Y. Bian, S. Contag Wise, J. Burnett, J. Coupar, X. Yang, Z. Chen, C. Van Waes, J. Burnett, J. Coupar, et al.. 2013. TGF-β and NF-κB signal pathway cross-talk is mediated through TAK1 and SMAD7 in a subset of head and neck cancers. *Oncogene.* 32:1549–1559. http://dx.doi.org/10.1038/onc.2012.171

Gordon, J.R. 2000. TGFβ1 and TNFα secreted by mast cells stimulated via the FcεRI activate fibroblasts for high-level production of monocyte chemoattractant protein-1 (MCP-1). *Cell. Immunol.* 201:42–49. http://dx.doi.org/10.1006/cimm.2000.1631

Greten, F.R., L. Eckmann, T.F. Greten, J.M. Park, Z.-W. Li, L.J. Egan, M.F. Kagnoff, and M. Karin. 2004. IKKβ links inflammation and tumorigenesis in a mouse model of colitis-associated cancer. *Cell.* 118:285–296. http://dx.doi.org/10.1016/j.cell.2004.07.013

Greten, F.R., M.C. Arkan, J. Bollrath, L.-C. Hsu, J. Goode, C. Miething, S.I. Göktuna, M. Neuenhahn, J. Fierer, S. Paxian, et al.. 2007. NF-κB is a negative regulator of IL-1β secretion as revealed by genetic and pharmacological inhibition of IKKβ. *Cell.* 130:918–931. http://dx.doi.org/10.1016/j.cell.2007.07.009

Hanahan, D., and L.M. Coussens. 2012. Accessories to the crime: functions of cells recruited to the tumor microenvironment. *Cancer Cell.* 21:309–322. http://dx.doi.org/10.1016/j.ccr.2012.02.022

Hong, S., C. Lee, and S.-J. Kim. 2007. Smad7 sensitizes tumor necrosis factor induced apoptosis through the inhibition of antiapoptotic gene expression by suppressing activation of the nuclear factor-κB pathway. *Cancer Res.* 67:9577–9583. http://dx.doi.org/10.1158/0008-5472.CAN-07-1179

Hoot, K.E., M. Oka, G. Han, E. Bottinger, Q. Zhang, and X.J. Wang. 2010. HGF upregulation contributes to angiogenesis in mice with keratinocyte-specific Smad2 deletion. *J. Clin. Invest.* 120:3606–3616. http://dx.doi.org/10.1172/JCI43304

Jung, D.W., Z.M. Che, J. Kim, K. Kim, K.Y. Kim, D. Williams, and J. Kim. 2010. Tumor-stromal crosstalk in invasion of oral squamous cell carcinoma: a pivotal role of CCL7. *Int. J. Cancer.* 127:332–344.

Karin, M. 2009. NF-κB as a critical link between inflammation and cancer. *Cold Spring Harb. Perspect. Biol.* 1:a000141. http://dx.doi.org/10.1101/cshperspect.a000141

Koliaraki, V., M. Roulis, and G. Kollias. 2012. Tpl2 regulates intestinal myofibroblast HGF release to suppress colitis-associated tumorigenesis. *J. Clin. Invest.* 122:4231–4242. http://dx.doi.org/10.1172/JCI63917

Koliaraki, V., M. Pasparakis, and G. Kollias. 2015. IKKβ in intestinal mesenchymal cells promotes initiation of colitis-associated cancer. *J. Exp. Med.* http://dx.doi.org/10.1084/jem.20150576

Lewis, M.P., K.A. Lygoe, M.L. Nystrom, W.P. Anderson, P.M. Speight, J.F. Marshall, and G.J. Thomas. 2004. Tumour-derived TGF-β1 modulates myofibroblast differentiation and promotes HGF/SF-dependent invasion of squamous carcinoma cells. *Br. J. Cancer.* 90:822–832. http://dx.doi.org/10.1038/sj.bjc.6601611

Liu, X., Q. Wang, G. Yang, C. Marando, H.K. Koblish, L.M. Hall, J.S. Fridman, E. Behshad, R. Wynn, Y. Li, et al.. 2011. A novel kinase inhibitor, INCB28060, blocks c-MET-dependent signaling, neoplastic activities, and cross-talk with EGFR and HER-3. *Clin. Cancer Res.* 17:7127–7138. http://dx.doi.org/10.1158/1078-0432.CCR-11-1157

Liu, Y., Q. Li, and L. Zhu. 2012. Expression of the hepatocyte growth factor and c-Met in colon cancer: correlation with clinicopathological features and overall survival. *Tumori.* 98:105–112.

Nakamura, T., K. Sakai, T. Nakamura, and K. Matsumoto. 2011. Hepatocyte growth factor twenty years on: Much more than a growth factor. *J. Gastroenterol. Hepatol.* 26(Suppl 1):188–202. http://dx.doi.org/10.1111/j.1440-1746.2010.06549.x

Ogura, N., M. Tobe, H. Sakamaki, H. Nagura, H. Hosaka, M. Akiba, Y. Abiko, and T. Kondoh. 2004. Interleukin-1β increases RANTES gene expression and production in synovial fibroblasts from human temporomandibular joint. *J. Oral Pathol. Med.* 33:629–633. http://dx.doi.org/10.1111/j.1600-0714.2004.00260.x

Öhlund, D., E. Elyada, and D. Tuveson. 2014. Fibroblast heterogeneity in the cancer wound. *J. Exp. Med.* 211:1503–1523.

Okunishi, K., M. Dohi, K. Fujio, K. Nakagome, Y. Tabata, T. Okasora, M. Seki, M. Shibuya, M. Imamura, H. Harada, et al.. 2007. Hepatocyte growth factor significantly suppresses collagen-induced arthritis in mice. *J. Immunol.* 179:5504–5513. http://dx.doi.org/10.4049/jimmunol.179.8.5504

Organ, S.L., and M.-S. Tsao. 2011. An overview of the c-MET signaling pathway. *Ther. Adv. Med. Oncol.* S7–S19. http://dx.doi.org/10.1177/1758834011422556

Orimo, A., P.B. Gupta, D.C. Sgroi, F. Arenzana-Seisdedos, T. Delaunay, R. Naeem, V.J. Carey, A.L. Richardson, and R.A. Weinberg. 2005. Stromal fibroblasts present in invasive human breast carcinomas promote tumor growth and angiogenesis through elevated SDF-1/CXCL12 secretion. *Cell.* 121:335–348. http://dx.doi.org/10.1016/j.cell.2005.02.034

Östman, A., and M. Augsten. 2009. Cancer-associated fibroblasts and tumor growth--bystanders turning into key players. *Curr. Opin. Genet. Dev.* 19:67–73.

Özdemir, B.C., T. Pentcheva-Hoang, J.L. Carstens, X. Zheng, C.-C. Wu, T.R. Simpson, H. Laklai, H. Sugimoto, C. Kahlert, S.V. Novitskiy, et al.. 2014. Depletion of carcinoma-associated fibroblasts and fibrosis induces immunosuppression and accelerates pancreas cancer with reduced survival. *Cancer Cell.* 25:719–734. http://dx.doi.org/10.1016/j.ccr.2014.04.005

Pang, G., L. Couch, R. Batey, R. Clancy, and A. Cripps. 1994. GM-CSF, IL-1α, IL-1β, IL-6, IL-8, IL-10, ICAM-1 and VCAM-1 gene expression and cytokine production in human duodenal fibroblasts stimulated with lipopolysaccharide, IL-1 alpha and TNF-α. *Clin. Exp. Immunol.* 96:437–443.

Pilling, D., A.N. Akbar, J. Girdlestone, C.H. Orteu, N.J. Borthwick, N. Amft, D. Scheel-Toellner, C.D. Buckley, and M. Salmon. 1999. Interferon-β mediates stromal cell rescue of T cells from apoptosis. *Eur. J. Immunol.* 29:1041–1050. http://dx.doi.org/10.1002/(SICI)1521-4141(199903)29:03<1041::AID-IMM

Ponzetto, C., A. Bardelli, Z. Zhen, F. Maina, P. dalla Zonca, S. Giordano, A. Graziani, G. Panayotou, and P.M. Comoglio. 1994. A multifunctional docking site mediates signaling and transformation by the hepatocyte growth factor/scatter factor receptor family. *Cell.* 77:261–271.

Proto, J.D., Y. Tang, A. Lu, W.C.W. Chen, E. Stahl, M. Poddar, S.A. Beckman, P.D. Robbins, L.J. Nidernhofer, K. Imbrogno, et al. 2015. NF-κB inhibition reveals a novel role for HGF during skeletal muscle repair. *Cell Death Dis.* 6:e1730.

Quante, M., S.P. Tu, H. Tomita, T. Gonda, S.S.W. Wang, S. Takashi, G.H. Baik, W. Shibata, B. Diprete, K.S. Betz, et al.. 2011. Bone marrow-derived myofibroblasts contribute to the mesenchymal stem cell niche and promote tumor growth. *Cancer Cell.* 19:257–272. http://dx.doi.org/10.1016/j.ccr.2011.01.020

Räsänen, K., and A. Vaheri. 2010. Activation of fibroblasts in cancer stroma. *Exp. Cell Res.* 316:2713–2722. http://dx.doi.org/10.1016/j.yexcr.2010.04.032

Rhim, A.D., P.E. Oberstein, D.H. Thomas, E.T. Mirek, C.F. Palermo, S.A. Sastra, E.N. Dekleva, T. Saunders, C.P. Becerra, I.W. Tattersall, et al. 2014. Stromal elements act to restrain, rather than support, pancreatic ductal adenocarcinoma. *Cancer Cell.* 25:735–747.

Schwitalla, S., A.A. Fingerle, P. Cammareri, T. Nebelsiek, S.I. Göktuna, P.K. Ziegler, O. Canli, J. Heijmans, D.J. Huels, G. Moreaux, et al.. 2013a. Intestinal tumorigenesis initiated by dedifferentiation and acquisition of stem-cell-like properties. *Cell.* 152:25–38. http://dx.doi.org/10.1016/j.cell.2012.12.012

Schwitalla, S., P.K. Ziegler, D. Horst, V. Becker, I. Kerle, Y. Begus-Nahrmann, A. Lechel, K.L. Rudolph, R. Langer, J. Slotta-Huspenina, et al.. 2013b. Loss of p53 in enterocytes generates an inflammatory microenvironment enabling invasion and lymph node metastasis of carcinogen-induced colorectal tumors. *Cancer Cell.* 23:93–106. http://dx.doi.org/10.1016/j.ccr.2012.11.014

Servais, C., and N. Erez. 2013. From sentinel cells to inflammatory culprits: cancer-associated fibroblasts in tumour-related inflammation. *J. Pathol.* 229:198–207.

Stein, U., W. Walther, F. Arlt, H. Schwabe, J. Smith, I. Fichtner, W. Birchmeier, and P.M. Schlag. 2009. MACC1, a newly identified key regulator of HGF-MET signaling, predicts colon cancer metastasis. *Nat. Med.* 15:59–67. http://dx.doi.org/10.1038/nm.1889

Toullec, A., D. Gerald, G. Despouy, B. Bourachot, M. Cardon, S. Lefort, M. Richardson, G. Rigaill, M.C. Parrini, C. Lucchesi, et al.. 2010. Oxidative stress promotes myofibroblast differentiation and tumour spreading. *EMBO Mol. Med.* 2:211–230. http://dx.doi.org/10.1002/emmm.201000073

Trusolino, L., A. Bertotti, and P.M. Comoglio. 2010. MET signalling: principles and functions in development, organ regeneration and cancer. *Nat. Rev. Mol. Cell Biol.* 11:834–848.

Valencia, T., J.Y. Kim, S. Abu-Baker, J. Moscat-Pardos, C.S. Ahn, M. Reina-Campos, A. Duran, E.A. Castilla, C.M. Metallo, M.T. Diaz-Meco, and J. Moscat. 2014. Metabolic reprogramming of stromal fibroblasts through p62-mTORC1 signaling promotes inflammation and tumorigenesis. *Cancer Cell.* 26:121–135. http://dx.doi.org/10.1016/j.ccr.2014.05.004

Vermeulen, L., F. De Sousa E Melo, M. van der Heijden, K. Cameron, J.H. de Jong, T. Borovski, J.B. Tuynman, M. Todaro, C. Merz, H. Rodermond, et al.. 2010. Wnt activity defines colon cancer stem cells and is regulated by the microenvironment. *Nat. Cell Biol.* 12:468–476. http://dx.doi.org/10.1038/ncb2048

Vougioukalaki, M., D.C. Kanellis, K. Gkouskou, and A.G. Eliopoulos. 2011. Tpl2 kinase signal transduction in inflammation and cancer. *Cancer Lett.* 304:80–89. http://dx.doi.org/10.1016/j.canlet.2011.02.004

Yan, X., Z. Liu, and Y. Chen. 2009. Regulation of TGF-βsignaling by Smad7. *Acta Biochim. Biophys. Sin. (Shanghai).* 41:263–272. http://dx.doi.org/10.1093/abbs/gmp018

Yang, L., Y. Pang, and H.L. Moses. 2010. TGF-β and immune cells: an important regulatory axis in the tumor microenvironment and progression. *Trends Immunol.* 31:220–227. http://dx.doi.org/10.1016/j.it.2010.04.002

Yin, J., J.H. Lee, J. Zhang, Z. Gao, V.Y. Polotsky, and J. Ye. 2014. Regulation of hepatocyte growth factor expression by NF-κB and PPARγ in adipose tissue. *Am. J. Physiol. Endocrinol. Metab.* 306:E929–E936. http://dx.doi.org/10.1152/ajpendo.00687.2013

Yucel-Lindberg, T., and G. Brunius. 2006. Epidermal growth factor synergistically enhances interleukin-8 production in human gingival fibroblasts stimulated with interleukin-1β. *Arch. Oral Biol.* 51:892–898. http://dx.doi.org/10.1016/j.archoralbio.2006.03.004

Zhang, J., L. Chen, M. Xiao, C. Wang, and Z. Qin. 2011. $FSP1^+$ fibroblasts promote skin carcinogenesis by maintaining MCP-1–mediated macrophage infiltration and chronic inflammation. *Am. J. Pathol.* 178:382–390. http://dx.doi.org/10.1016/j.ajpath.2010.11.017

Zheng, B., Z. Zhang, C.M. Black, B. de Crombrugghe, and C.P. Denton. 2002. Ligand-dependent genetic recombination in fibroblasts: a potentially powerful technique for investigating gene function in fibrosis. *Am. J. Pathol.* 160:1609–1617. http://dx.doi.org/10.1016/S0002-9440(10)61108-X